Pergamon

Int. J. Heat Mass Transfer. Vol. 37, No. 11, pp. 1631–1640, 1994

0017-9310/94 $7.00+0.00

0017-9310(93)E0105-P

Laminar convective heat transfer in a horizontal isothermal tube for high Rayleigh numbers

G. J. HWANG and H. C. LAI

Department of Power Mechanical Engineering, National Tsing Hua University, Hsinchu, Taiwan, 30043, R.O.C.

(*Received* 27 *September* 1993 *and in final form* 1 *December* 1993)

Abstract—Laminar mixed convection heat transfer in a horizontal isothermal cooled tube for high Rayleigh numbers and Prandtl numbers is investigated numerically in the present study. The inlet fluid with a fully developed inlet velocity and a constant inlet temperature T_0 is cooled in the tube with a constant wall temperature T_w. Variation of the fluid and wall temperature difference and the heat transfer are governed by the Rayleigh number and the Graetz number. To achieve the high Rayleigh number solution in a sufficiently long range of z, a robust scheme of weighting function for solving the energy equation and a control volume method for evaluating the wall temperature gradient are employed. The varying Nu with $Ra = 0 \sim 5 \times 10^8$ in the range of $z = 0$–0.8 is obtained. This extends the solution to three orders higher in Ra and one order longer in z than those in the literature. Several axial positions characterizing the Nusselt number curve for each Ra are identified and correlated. Comparisons of Nu with the existing experimental data for Ra in the orders of 10^3–10^8 are made.

1. INTRODUCTION

THE MIXED convection flow in a horizontal isothermal tube is three dimensional and it is hard to analyze theoretically. Thus, the early studies of the mixed convection flow in horizontal isothermal tubes were confined to the experimental works for different fluids with discrete Prandtl-numbers. Notable examples are the studies by Colburn [1] in air, water, and light oils; Kern and Othmer [2] in three different oils; Eubank and Proctor [3] in petroleum and oils; Oliver [4] in water, ethyl alcohol, and 80:20 glycerol–water; Brown and Thomas [5] in water; and Depew and August [6] in water, ethyl alcohol, and 80 : 20 glycerol–water. From the available data, correlations of the important parameters of the Nusselt, Graetz, Grashof and Prandtl numbers are obtained with uncertainty of about $\pm 40\%$. This value suggests immediately the difficulty of the problem and the need for the analysis of the heat transfer mechanism. It should be noted that all the correlations were derived under the condition of hydrodynamically fully developed flow at the inlet of heating or cooling section.

Cheng *et al.* [7] first carried out the order of magnitude analysis for this problem, and found that the inertia terms in the momentum equation and axial conduction term in the energy equation can be neglected when Pr 1 and $Pe > 100$. The assumption of large Pr and Pe made the marching numerical solution at each cross-section possible. The theoretical studies before Cheng *et al.* [7] have been confined to the fully developed region of a uniform-heat-flux pipe, e.g. the perturbation–expansion solutions of Morton [8] and Faris and Viskanta [9], and the numerical solutions of Siegwarth and Hanratty [10] and Newell and Bergles [11]. Morton [8] got his perturbation equations with Rayleigh number as a perturbation parameter by assuming a constant axial temperature and pressure gradients and extended the series to Rayleigh number of about 10^3. Van Dyke [12] employed the Domb–Sykes plot and the Euler transformation to extend the Morton's series for Rayleigh number up to 10^6.

In the past two decades, after Cheng *et al.* [7], almost all the numerical studies for mixed convection in horizontal tubes employed the large Pr assumption. Heiber and Sreenivasan [13] carried out a theoretical analysis for mixed convection in an isothermally heated horizontal pipe with a uniform axial velocity profile at the pipe inlet for a large Pradtl number fluid. Ou and Cheng [14] obtained the numerical solutions of horizontal tubes with constant wall temperature for Ra up to 10^5 by using central difference for the convection terms. Hwang and Lin [15] employed Patankar's power law scheme, boundary–vorticity method and Du Fort–Frankel method to solve the same problem for $z = 0 \sim 0.1$ with Ra up to 10^6 and found that, for $Ra \geqslant 5 \times 10^5$, oscillatory flow patterns of one-pair and two-pairs of counter rotating vortices appear along the axial direction. According to their result, the appearance of the two-pair vortices decreases the heat transfer rate. It is also noted that two values of Nusselt numbers obtained from local wall temperature gradient and axial energy balance used in refs. [7, 14, 15] deviate with each other for $Ra \geqslant 5 \times 10^5$.

In practical engineering applications, the mixed convection flows with high Ra are frequently encountered. For example, the Ra value for glycol is about

NOMENCLATURE

a tube radius
k thermal conductivity
K a factor defined in equation (17)
g gravity
Gr Grashof number
Gz Graetz number, $Gz = 1/z$
M, N number of meshes
Nu_1, Nu_2 Nusselt numbers defined in equations (8) and (9)
$P(R, \phi), p$ pressure derivation due to secondary flow, and the dimensionless P
Pe Peclet number, $RePr$
R, ϕ, Z cylindrical coordinates
r, ϕ, z dimensionless cylindrical coordinates, $z = Z/2aRePr$
Ra Rayleigh number, $g\beta(T_0 - T_w)a^3/\alpha\nu$
Re Reynolds number, $2a\overline{W}_f/\nu$
Sh Sherwood number
T, T_0, T_w local temperature, uniform inlet temperature and constant wall temperature
U, V, W velocity components in R, ϕ and Z directions, respectively
u, v, w dimensionless velocity in r, ϕ and z directions, respectively
$\overline{W}_f$ average axial velocity
z_c position of free convection effect based on 2% deviation from that of Graetz solution
z_s position of maximum stream function
z_{np} position of peak Nusselt number
z_f position of full development.

Greek symbols
α thermal diffusivity
β thermal expansion coefficient
δ, Δ difference quantity
ε relative error
θ dimensionless temperature
μ dynamic viscosity
ν kinematic viscosity
ξ dimensionless vorticity
ρ density
ψ dimensionless stream function
∇^2 dimensionless Laplace operator, $(1/r)(\partial/\partial r)(r\,\partial/\partial r) + (1/r^2)(\partial^2/\partial\phi^2)$.

Subscripts
b bulk quantity
E, W, N, S, P grid points
f fully developed quantity
i, j nodal points
0 quantity at $z = 0$
w condition at wall.

Superscripts
p previous axial step
mean value.

1×10^8 in a 4 cm radius pipe with 100°C temperature difference. In order to facilitate the industrial applications, more analysis for high Ra is required. The attempt of the present study is to solve the laminar mixed convection heat transfer in an isothermal heated horizontal tube numerically for high Rayleigh numbers. To achieve the high Rayleigh number solution in a sufficiently long range of z, a weighting function scheme [16, 17] and boundary–vorticity technique [18] are employed for solving the energy equation, and a control volume method developed in the present study is used to evaluate the wall temperature gradient for the Nusselt number.

2. THEORETICAL ANALYSIS

2.1. *Problem description*

It is well known that the Graetz solution is valid for pure forced convection heat transfer in a horizontal isothermal cooled tube. When the effect of natural convection is taken into account, the Graetz solutions are no longer applicable for $Ra \geqslant 10^3$ [7, 13–15]. In the present study, the tube wall temperature is lower than that of the inlet fluid; the induced buoyant forces, due to the temperature gradient of fluid, cause a secondary flow circulation upward at the tube center and downward near the wall vicinity. The combination of the forced main flow and the secondary flow sets up the forward moving spirals. The heat transfer coefficient is known to be enhanced by the consequent mixing due to the secondary flow. Since the two spiral-like motion is symmetrical about the Y-axis, the geometry we calculate here is half circle only. The physical configuration is shown in Fig. 1. The flow enters the tube with a fully developed parabolic vel-

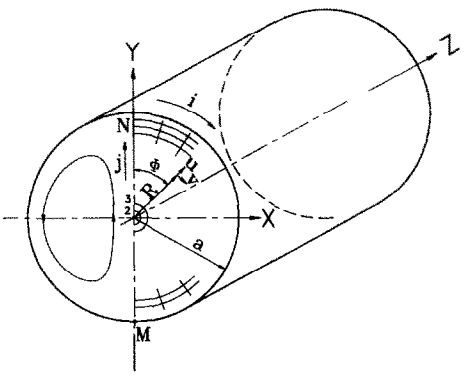

FIG. 1. Physical configuration.

ocity and a uniform temperature, T_0. To facilitate the analysis, the following basic assumptions are made:

(1) steady, laminar, incompressible, and no viscous dissipation;

(2) constant thermophysical properties and the validity of Boussinesq approximation;

(3) small Grashof number, and large Prandtl and Peclet numbers.

With the foregoing assumptions, the secondary flow velocities are small compared with the axial main flow velocity, and make no effect on the main flow velocity profile. The small secondary flow velocities are expected to be symmetry with respect to the vertical center plane and may have a significant effect on heat transfer via the amplification of the large Prandtl number. Physically, the large fluid viscosity suppresses the inertia terms in the momentum equations, and the small thermal diffusivity gives a relatively large convection term over the diffusions term in energy equation.

The following dimensionless transformations and parameters are introduced

$$r = \frac{R}{a}, \quad z = \frac{Z}{2a\,Re\,Pr},$$

$$u = \frac{U}{\left(\frac{\alpha}{a}\right)Ra}, \quad v = \frac{V}{\left(\frac{\alpha}{a}\right)Ra},$$

$$w_f = \frac{W_f}{\overline{W}_f} = 2(1-r^2), \quad p = \frac{P}{\left(\frac{Gr\rho v^2}{a^2}\right)}$$

$$\theta = \frac{T-T_w}{T_0-T_w}, \quad Ra = Pr\,Gr = \frac{g\beta(T_0-T_w)a^3}{\alpha v}.$$

According to refs. [7, 14], the dimensionless governing equations are:

$$\frac{1}{r}\frac{\partial}{\partial r}(ru) + \frac{1}{r}\frac{\partial v}{\partial \phi} = 0 \tag{1}$$

$$-\frac{\partial p}{\partial r} + \left(\nabla^2 u - \frac{2}{r^2}\frac{\partial v}{\partial \phi} - \frac{u}{r^2}\right) + \theta\cos\phi = 0 \tag{2}$$

$$-\frac{1}{r}\frac{\partial p}{\partial \phi} + \left(\nabla^2 v - \frac{2}{r^2}\frac{\partial u}{\partial \phi} - \frac{v}{r^2}\right) + \theta\sin\phi = 0 \tag{3}$$

$$Ra\left(u\frac{\partial\theta}{\partial r} + \frac{v}{r}\frac{\partial\theta}{\partial\phi}\right) + \frac{w_f}{4}\frac{\partial\theta}{\partial z} = \nabla^2\theta \tag{4}$$

where

$$\nabla^2 = \frac{1}{r}\frac{\partial}{\partial r}\left(r\frac{\partial}{\partial r}\right) + \frac{1}{r^2}\frac{\partial^2}{\partial\phi^2}.$$

It is seen that the cross sectional velocity components u and v from equations (2) and (4), respectively, do not affect the fully-developed main flow velocity w_f, due to weak secondary motion. Therefore, only a two-dimensional continuity equation is required. The developments of components u and v depend solely on the buoyancy force at each cross section. Equation (4) tells physically the mechanism of the transport of heat. The heat is carried to the cross section by the axial convection, and then carried away convectively in the r- and ϕ- directions and finally conducted to the tube wall.

One can combine equations (2) and (3) to drop the pressure terms by taking a cross-differentiation. Dimensionless stream function ψ and vorticity ξ are defined and the final governing equations in dimensionless forms are:

$$\nabla^2\theta + \frac{Ra}{r}\left(\frac{\partial\psi}{\partial r}\frac{\partial\theta}{\partial\phi} - \frac{\partial\psi}{\partial\phi}\frac{\partial\theta}{\partial r}\right) - \frac{w_f}{4}\frac{\partial\theta}{\partial z} = 0 \tag{5}$$

$$\nabla^2\xi = -\left(\frac{\partial\theta}{\partial r}\sin\phi + \frac{1}{r}\frac{\partial\theta}{\partial\phi}\cos\phi\right) \tag{6}$$

$$\nabla^2\psi - \xi \tag{7}$$

where

$$u = \frac{1}{r}\frac{\partial\psi}{\partial\phi}, \quad \text{and} \quad v = -\frac{\partial\psi}{\partial r}.$$

It is obvious that both the vorticity transport equation (6) and stream function equation (7) are of elliptic type and the energy equation (5) is of parabolic. The corresponding initial and boundary conditions are:

$$\theta(r, \phi, 0) = 1 \qquad \text{at inlet}$$

$$\theta(r, \phi, 1) = \psi(r, \phi, 1) = \frac{\partial\psi(r, \phi, 1)}{\partial r} = 0$$

on the tube wall

$$\frac{\partial\theta(r, \phi, z)}{\partial\phi} = \psi(r, \phi, z) = \xi(r, \phi, z) = 0$$

along the vertical center plane.

From the above boundary conditions, one finds that the boundary condition of ξ at $r = 1$ is missing but there is one more boundary condition of ψ at $r = 1$. Thus one is able to solve equations (6) and (7) simultaneously by using of the boundary–vorticity method [18].

2.2. *Nusselt number*

Due to the invariant axial main flow velocity, friction factor is a constant and will not be discussed here. The variation of heat transfer coefficient significantly affected by the buoyancy forces can be evaluated by using the local wall temperature gradient and axial temperature gradient. One can derive the local Nusselt number, $Nu = (2a)h/k$, as written in ref. [14].

$$Nu_1 = -\frac{2}{\pi\theta_b}\int_0^\pi \left(\frac{\partial\theta}{\partial r}\right)_{r=1} d\phi \tag{8}$$

$$Nu_2 = -\frac{1}{2\pi\theta_b}\int_0^{\pi}\int_0^1 \frac{\partial\theta}{\partial z} w_f r \, dr \, d\phi \qquad (9)$$

where

$$\theta_b = \frac{2}{\pi}\int_0^{\pi}\int_0^1 w_f \theta r \, dr \, d\phi$$

is the dimensionless bulk temperature.

The wall temperature gradient of equation (8) was computed by using a three-point backward finite difference scheme,

$$\left(\frac{\partial\theta}{\partial r}\right)_{i,j} = \frac{3\theta_{i,j} - 4\theta_{i-1,j} + \theta_{i-2,j}}{2\Delta r},$$

to evaluate Nu_1 in the previous studies [7, 14]. This induces a large deviation from the local Nusselt number of Nu_2 for $Ra \sim O(10^6)$. In order to overcome this difficulty, the present study develops an improved numerical scheme for evaluating the wall temperature gradient. By the conservation principles of energy in a control volume near the wall as depicted in Fig. 2, one has

$$E1 - E2 + E3 - E4 + E5 - E6 = 0 \qquad (10)$$

where

$$E1 = -kR_s\Delta\phi\Delta Z\left(\frac{\partial T}{\partial R}\right)_{R=R_s} + R_s\Delta\phi\Delta Z U_s \rho C_p T_s$$

$$E2 = -ka\Delta\phi\Delta Z\left(\frac{\partial T}{\partial R}\right)_{R=a}$$

$$E3 = -k\Delta R\Delta Z\left(\frac{\partial T}{R_w\partial\phi}\right)_{\phi=\phi_w} + \Delta R\Delta Z V_w \rho C_p T_w$$

$$E4 = -k\Delta R\Delta Z\left(\frac{\partial T}{R_e\partial\phi}\right)_{\phi=\phi_e} + \Delta R\Delta Z V_e \rho C_p T_e$$

$$E5 = R_p\Delta\phi\Delta R W_p \rho C_p T_p$$

$$E6 = R_{pp}\Delta\phi\Delta R W_{pp}\rho C_p T_{pp}.$$

From the conservation of mass, one gets

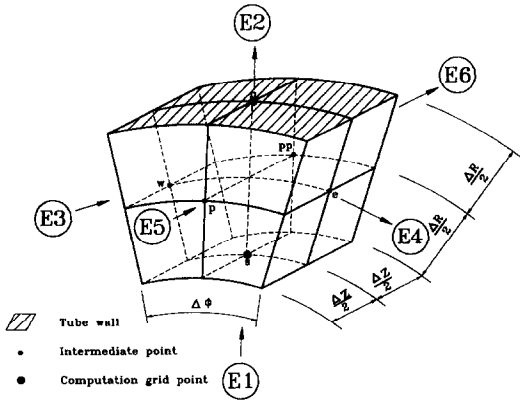

FIG. 2. Control volume for evaluating wall temperature gradient.

$$\rho R_s\Delta\phi\Delta Z U_s + \rho\Delta R\Delta Z V_w - \rho\Delta R\Delta Z V_e + \rho R_p\Delta\phi\Delta R W_p - \rho R_{pp}\Delta\phi\Delta R W_{pp} = 0. \qquad (11)$$

One obtains the following dimensionless form after a rearrangement,

$$\left(\frac{\partial\theta}{\partial r}\right)_{r=1} = r_s\left(\frac{\partial\theta}{\partial r}\right)_{r=r_s} - Rar_s u_s\theta_s + \frac{\Delta r}{r_w\Delta\phi}\left[\left(\frac{\partial\theta}{\partial\phi}\right)_{\phi=\phi_w} - \left(\frac{\partial\theta}{\partial\phi}\right)_{\phi=\phi_e}\right] + \frac{\Delta r}{\Delta\phi} Ra(v_e\theta_e - v_w\theta_w) + \frac{1}{4}\frac{r_p\Delta r}{\Delta z} w_p(\theta_{pp} - \theta_p). \qquad (12)$$

Central finite difference schemes are used for the derivatives on the right hand side of equation (12). The quantities with lower case subscripts e and w are obtained from the average of four neighbor grid points.

3. METHOD OF SOLUTION

3.1. *Discretization of equations*

The weighting function scheme [16, 17] is used to discretize the governing equations here. Since all of the governing equations are elliptic type in r and ϕ derivatives, we can discrete equations (5), (6) and (7) as

$$A_E\theta_E + A_W\theta_W + A_N\theta_N + A_S\theta_S = A_P\theta_P + \frac{\partial\theta}{\partial z} \qquad (13)$$

$$B_E\xi_E + B_W\xi_W + B_P\xi_P + B_N\xi_N + B_S\xi_S = B_R \qquad (14)$$

$$B_E\psi_E + B_W\psi_W + B_P\psi_P + B_N\psi_N + B_S\psi_S = b_R \qquad (15)$$

where the coefficients are listed in the Appendix.

By introducing a factor K [16], the axial derivative of equation (13) at the present time step is discretized as

$$\frac{\partial\theta}{\partial z} = \frac{\theta - \overline{\theta^p}}{K\Delta z}, \quad \text{and} \quad \overline{\theta^p} = \theta^p + (1-K)\Delta z\left.\frac{\partial\theta}{\partial z}\right|^p \qquad (16)$$

where the superscript p denotes the value at the previous step. When $K = 1$, equation (16) is a backward difference formula, and equation (13) becomes a fully implicit scheme. When $K = 0.5$, an average slope is used, and equation (13) becomes the Crank–Nicolson scheme. For $0.5 < K < 1$, different weighting of gradients for the present and previous steps can be attained.

In the present study, the factor K is selected from grid to grid in a cross section as

$$K = 1 + (\eta - 1.5)\eta^2 \quad \text{when} \quad \eta = \frac{s}{f} \leqslant 1 \qquad (17)$$

$$K = 0.5 \quad \text{when} \quad \eta = \frac{s}{f} \geqslant 1$$

where f is a factor, assume $f = 0.1$ is used in the present study, and s is ratio of present temperature derivative at the computation to that at the previous step, $s = (\partial\theta/\partial z)/(\partial\theta/\partial z)^p$. In the region near the inlet, the

value K close to 1 gives a more stable solution, the value close to 0.5 offers a more accurate solution and is used near the fully developed region. Equation (5) is singular at the tube center, $r = 0$, and the discretized equation (15) can not be used. In order to avoid the singularity, a finite difference equation based on Cartesian coordinates is used, and the energy equation (5) is solved explicitly at the center point.

3.2. *Numerical methods*

Energy equation (5) is solved for temperature by a step by step marching technique from the tube inlet to the fully developed region. Local values of ψ and ξ are then solved by the resulting local temperature. Near the tube inlet, the axial gradient of temperature near the tube wall is large and a very small axial step is required for an accurate solution. In the downstream region, temperature variation is not distinct and a larger step is allowable. Thus, a continuously increasing unequal axial step is used in the present study. For $Ra \leqslant 10^6$, the axial step sizes are varied from $\Delta z = 1 \times 10^{-7}$ near the entrance to 3×10^{-4} for $z \geqslant 0.2$, the step sizes for $10^6 < Ra \leqslant 10^7$ are $\Delta z = 10^{-8} \sim 10^{-4}$ and for $Ra > 10^7$ the step sizes are $\Delta z = 10^{-8} \sim 5 \times 10^{-5}$.

As mentioned previously, the boundary condition of vorticity ξ at r = 1 is not available. Therefore, the vorticity transport equation (6) should be solved simultaneously with equation (7) by using a line iteration and the boundary vorticity method [18].

The numerical procedure for solving equations (5)–(7) with the associated boundary conditions is listed below.

1. Set $\theta - 1 = \xi = \psi = u = v = 0$ at $z = 0$.
2. Apply ξ, ψ, u and v at the previous axial step, and solve equation (5) for the temperature at the present step.
3. Solve the vorticity transport and the stream–vorticity equations (6) and (7) simultaneously by using the boundary vorticity method. A relaxation factor of 1.74 is tested and the iteration of ξ and ψ at present axial position is terminated when the stream function ψ satisfies the criterion.

$$\varepsilon = \frac{\text{Max} \mid \psi_{i,j}^{k+1} - \psi_{i,j}^{k} \mid}{\text{Max} \mid \psi_{i,j}^{k+1} \mid} < 10^{-4}.$$

4. Repeat steps 2 and 3 until $z = 0.8$ is reached.

A uniform grid system is applied in the present study. Grid size tests were carried out for $Ra = 10^6$, 5×10^6, 10^7, 10^8 and 5×10^8. Tables 1 and 2 show the results of the typical grid test for $Ra = 10^7$ and 5×10^8, respectively. In the present study, 31×31 ($N \times M$) grids are used for the cases of $Ra \leqslant 10^6$, 41×31 grids for $Ra = 5 \times 10^6$, 51×31 grids for $Ra = 10^7$, 71×31 grids for $Ra = 5 \times 10^7$ and 10^8, and 101×31 grids for $Ra = 5 \times 10^8$. It is seen in Table 1 that the differences in Nu_1 between 51×31 and finer grid system are around 1%. For $Ra = 5 \times 10^8$, this value is relaxed up to around 3% as shown in Table 2. To verify further the accuracy of the values of Nu_1 by the control volume method, the values of Nu numbers obtained by using the control volume method, 3-point finite difference scheme and axial temperature gradient as shown in equation (9) are compared as shown in Table 3. It is seen that the present control volume method drastically reduces the difference with that from equation (9) as compared with that from 3-point finite difference scheme. In the present study, Nu_1 obtained by using the control volume method is used for the present study. Note that the evaluation of Nu_2 is based on equation (9)

4. RESULTS AND DISCUSSION

To depict the typical axial development of flow and temperature fields for high Ra Fig. 3 shows the streamline patterns and isotherms at various axial locations for $Ra = 10^8$. It is seen that the isotherms are concentric circles in the beginning of the entrance region and are gradually distorted upward near the tube bottom and center further downstream due to upward buoyancy flow effects. High temperature fluid in the core region moves upward and the cooled fluid near wall moves downward. Therefore, the isotherms are closely spaced near the top of the tube and sparsely spaced near the tube bottom. This indicates that there is high wall heat flux in the upper semicircle and low heat flux in the lower semicircle. When the thermally fully developed region is reached, the buoyancy effect diminishes, and the isotherms return to the pattern of concentric circles with constant spacing.

Since the secondary flow is independent of the main flow velocity component, the secondary flow pattern depends only on the local temperature field. As shown in Fig. 3, the flow patterns near the inlet and in the fully developed region are symmetric with respect to the horizontal center plane, because of small buoyancy effects. In other locations, the symmetry is lost due to the distortion of isotherms. Also, from Fig. 3, one finds that the location of vortex center representing the maximum stream function is moved downward from the center plane first and then moved upward to the upper semicircle. Finally, when the fully developed region is reached, it is restored to the center plane. The variation of the location of the vortex center with the corresponding z_s and z_{np} is displayed in Fig. 4. For lower Ra, the center moves around in the vicinity of the horizontal center plane. For higher Ra, the center moves further to the upper part of circular tube, and then moves back to the horizontal center plane when the thermal fluid flow is fully developed.

Figure 5 shows the variation of local Nusselt number with the Graetz number (inverse of dimensionless z) for Ra ranging from 0 to 5×10^8. With the effect of buoyancy, the Nusselt number deviates from the curve of Graetz solution and when the fully developed region is reached, the Nusselt number merges with the

Table 1. Numerical experiment of grid systems for $Ra = 10^7$

z	0.00001	0.00005	0.0001	0.0005	0.001	0.005
$(N \times M)$						
41×31	54.43†	48.66	47.97	47.52	48.05	47.33
51×31‡	52.88	46.88	46.10	45.10	45.35	45.80
51×41	52.89	46.85	46.04	45.01	45.61	46.50
61×31	52.06	46.23	45.43	45.24	44.38	45.34

†These values are Nu_1 and evaluated by using equations (8) and (12).
‡The grid size is used in the present study.

Table 2. Numerical experiment of grid systems for $Ra = 5 \times 10^8$

z	0.00001	0.00005	0.0001	0.0005	0.001	0.005
$(N \times M)$						
91×31	138.35†	136.22	136.33	145.18	—	—
101×31‡	133.28	130.4	130.02	136.93	141.61	88.51
101×41	133.06	130.04	129.64	137.23	142.81	91.00
111×31	130.12	126.77	125.99	131.41	136.01	88.53

†These values are Nu_1 and evaluated by using equations (8) and (12).
‡The grid size is used in the present study.

Table 3. Comparison of $[(Nu_1 - Nu_2)/Nu_2] \times 100\%$

z	0.0001	0.001	0.01	0.1
$Ra = 10^4$	0.54† (6.95)‡	0.12 (0.6)	0.16 (0.95)	0.09 (0.03)
$Ra = 10^6$	3.26 (13.99)	3.70 (15.09)	3.81 (9.82)	0.15 (0.34)
$Ra = 10^8$	5.21 (19.54)	1.91 (18.06)	2.78 (7.52)	0.04 (0.03)

†The Nu_1 are from the control volume method as shown in equation (12).
‡The Nu_1 used are from 3-point finite difference scheme.

curve again. In contrast to the results of previous investigations, the present study achieves the solution for Ra up to about 2 or 3 orders of magnitude higher than the previous ones. Wide ranges of Gz are found for almost constant value of Nusselt number. The constant value of Nu can be correlated by $Nu_1 = 0.626\ Ra^{0.269}$ with an error of 1.4% from the present numerical data for $Ra \geqslant 10^5$. Experimental data of Hwang and Chen [20] in electrochemical system are also plotted for comparison. The Sherwood number Sh in mass transfer is analogous to the Nusselt number in heat transfer. There is a root mean square difference of 17% between the experimental data and the interpolation data of present results for $Ra = 2.69 \times 10^7$ and 17.5% for $Ra = 2.628 \times 10^8$.

Although the comparison was made in the literature between the numerical and experimental data for $Ra \leqslant 10^6$, Fig. 6 also makes a comparison of Nusselt number with data from refs. [6, 19] and Oliver [4]. The root mean square difference for data of Depew [6] are within 17%. Especially, an excellent agreement is found for water with $Ra = 1.06 \sim 1.16 \times 10^5$ and for ethyl and alcohol solution with $Ra = 1.00 \sim 1.76 \times 10^6$. The root mean square differences are 6.5% for the former case and 4.5% for the latter. For data of Depew and Zenter [19] and Oliver [4], good agreement is also found.

The variation of bulk temperature is shown in Fig. 7. One finds that all the bulk temperature curves start from $\theta_b = 1$ at $z = 0$ and are parallel with each other in the fully developed region. The slope of these lines is identical to that of Graetz solution. Since all the lines are regularly spaced in the fully developed region, the bulk temperature $\theta_b(Ra,z)$ can be correlated as $\theta_b(Ra,z) = 0.819 \exp(7.54 - 0.92 \times \ln(Ra) - 14.6z)$ for $Ra \geqslant 5 \times 10^5$. Some data of the correlation are plotted in Fig. 7 for comparison. The root mean square difference of correlated data and that of the present study is about 2.7%.

Since the present study extends the solution to three orders higher in Ra and one order longer in z, one is able to identify some important axial positions characterizing the Nusselt number curve, as shown in Fig 8. z_c indicates the position with 2% higher in Nu than that of pure forced convection. z_s shows the position with maximum value of stream function. It is interesting to see that the region with constant Nu also starts from this position region. z_{ap} depicts the position

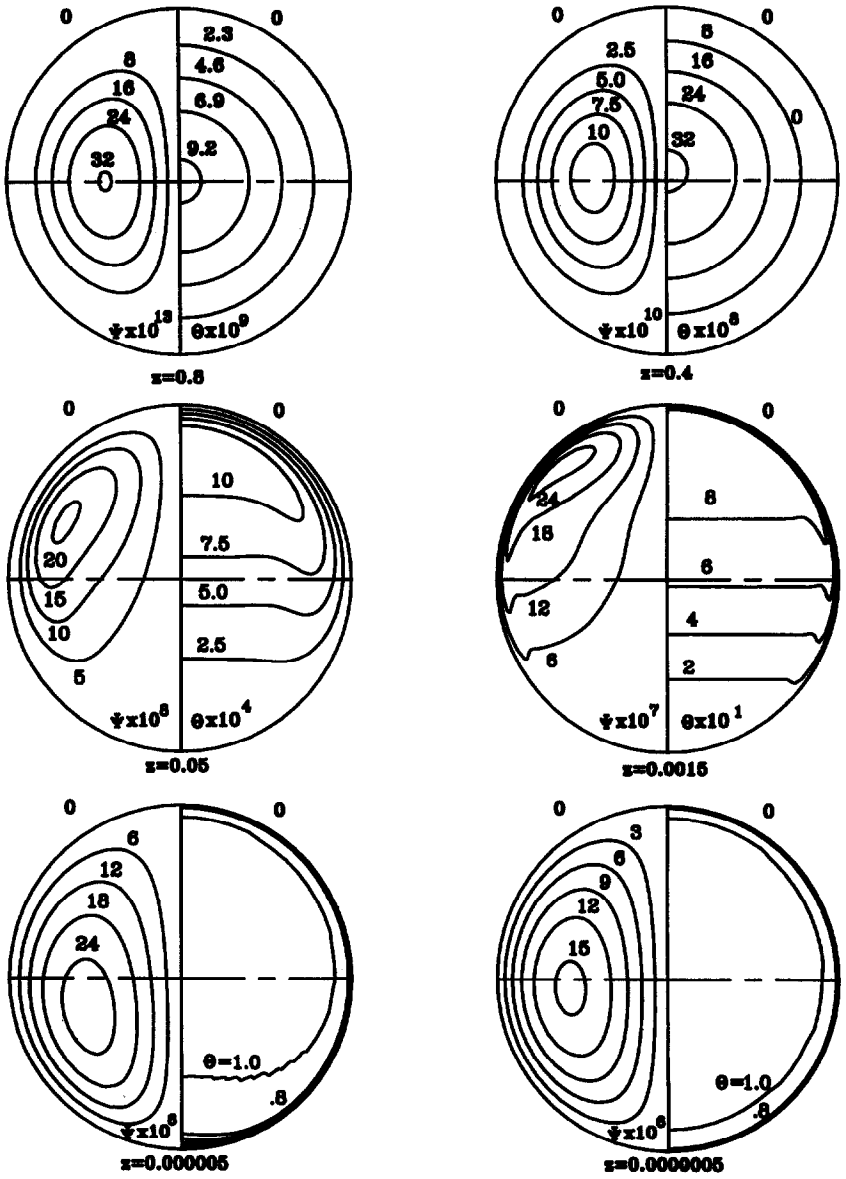

FIG. 3. Development of streamline patterns and isotherms for $Ra = 10^8$.

with peak value in the Nusselt number. z_f is the position with a fully developed Nusselt number. When $z < z_c$, the Graetz solution is valid. At $z > z_c$, the Nu is declining because the entrance effect is greater than the natural convection effect in this region. When $z > z_s$, the natural convection overcomes the decrease of entrance effect. The Nu is almost invariant with z until the location z_{np} for the peak Nu number with largest natural convection effect is reached. After z_{np}, both the natural convection and the entrance effect are declining, the Nu drops rapidly. When $z = z_f$ is reached, the Nusselt number merges with the fully developed value, and both the natural convection effect and entrance effect vanish. In Fig. 8, the open circles are points taken from the numerical data, and the solid lines are the linear correlation of the data points. They are

$$z_c = 2.84\, Ra^{-0.820}$$

$$z_s = 2.85\, Ra^{-0.720}$$

$$z_{np} = 0.248\, Ra^{-0.275}.$$

The root mean square difference predicted by the correlations are within 9.2% for z_c, 4.8% for z_s, and 5.7% for z_{np}. The solid circles are the points for the entrance lengths required to achieve the fully developed $Nu = 3.6$. The values of z_f vary from 0.2 for $Ra = 10^3$ to 0.36 for $Ra \geqslant 5 \times 10^7$. For $z \geqslant z_f$ the fully developed region or $Nu = 3.6$ is achieved for all Ra.

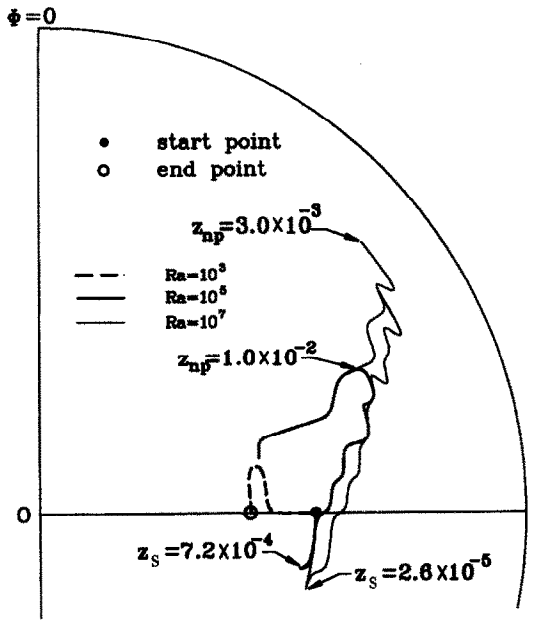

FIG. 4. Variation of location of maximum stream function.

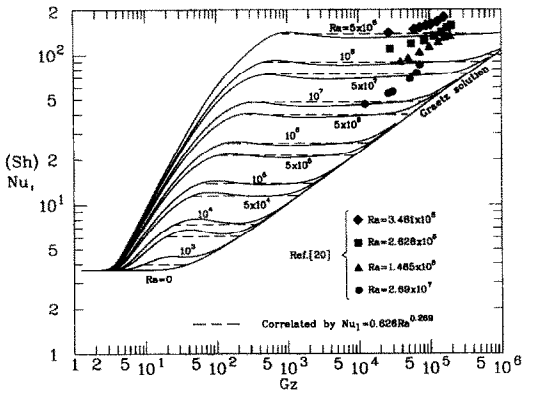

FIG. 5. Local Nusselt number variation with Gz for $Ra = 0$–5×10^8 and comparison with experimental data.

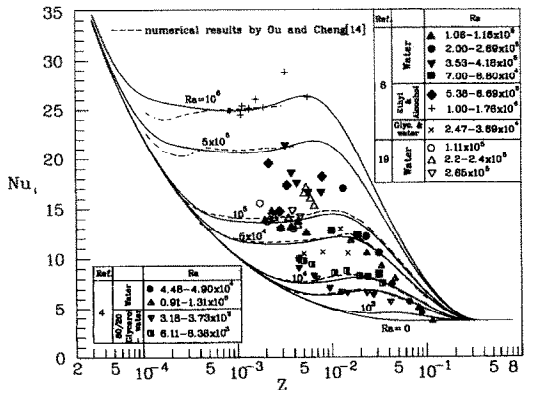

FIG. 6. Comparison of local Nusselt number with experimental data for $Ra = 0$–10^6.

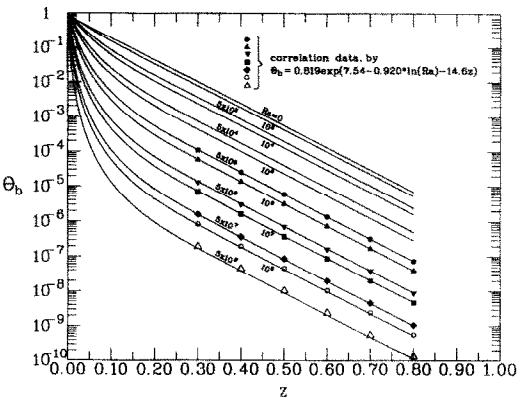

FIG. 7. Bulk temperature θ_b variation with z.

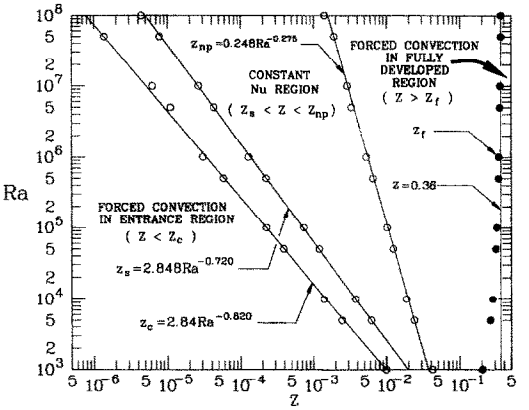

FIG. 8. The axial positions characterizing the Nu curves.

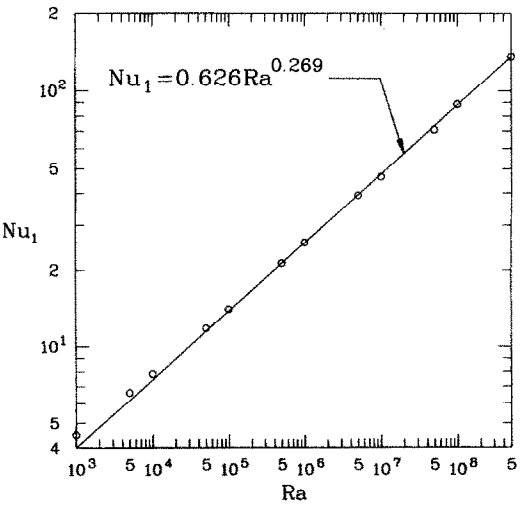

FIG. 9. Nusselt number variation in $z_s \leqslant z \leqslant z_{np}$.

It is interesting to see in Figs. 5 and 6 that the values of Nu in the region $z_s \leqslant z \leqslant z_{np}$ are almost constant, and the curves of Nu are almost regularly spaced for high Ra. The Nusselt number correlation in this region is shown in Fig. 9. The open circles are points taken numerically at the arithmatic average of the peak and lower values of the Nusselt number. The correlation is $Nu_1 = 0.626\, Ra^{0.269}$ and only a few percent difference is observed.

5. CONCLUSIONS

1. By utilization of weighting function scheme and the control volume method for evaluation of Nu, the present study obtains Nu for Ra up to 5×10^8 in a range of $z = 0$–0.8. This extends the solution to three orders higher in Ra and one order longer in z than those in the literature.

2. As a result of this study, several axial positions characterizing the Nusselt number curve for each Ra are identified. The variations of z_c, z_s, z_{np} and z_f with Rayleigh numbers are correlated.

3. The Nusselt numbers are found almost invariant in the range between z_s and z_{np}. A correlation of Nu in this range with Ra is also made, and only a few percent deviation is observed.

REFERENCES

1. A. P. Colburn, A method of correlating forced convection heat transfer data and a comparison with fluid friction, *Trans. Am. Inst. Chem. Engrs* **29,** 174–210 (1993).
2. D. Q. Kern and D. F. Othmer, Effect of free convection on viscous heat transfer in horizontal tubes, *Trans. Am. Inst. Chem. Engrs* **39,** 517–555 (1943).
3. C. C. Eubank and W. S. Proctor, MS Thesis in Chemical Engineering, M. I. T., Cambridge, MA (1951).
4. D. R. Oliver, The effect of natural convection on viscous flow heat transfer in horizontal tubes, *Chem. Engng Sci.* **17,** 335–350 (1962).
5. A. R. Brown and M. A. Thomas, Combined free and forced convection heat transfer for laminar flow in horizontal tubes, *J. Mech. Engng Sci.* **7**(4), 440–448 (1965).
6. C. A. Depew and S. E. August, Heat transfer due to combined free and forced convection in a horizontal and isothermal tubes, *J. Heat Transfer* **93,** 380–384 (1971).
7. K. C. Cheng, S. E. Hong and G. J. Hwang, Buoyancy effect on laminar heat transfer in the thermal entrance region of horizontal rectangular channels with uniform wall heat flux for large Prandtl number fluid, *Int. J. Heat Mass Transfer* **15,** 1819–1836 (1972).
8. B. R. Morton, Laminar convection in uniformly heated horizontal pipes at low Rayleigh number, *Q. J. Mech. Appl. Maths.* **12,** 410–420 (1959).
9. G. N. Faris and R. Viskanta, An analysis of laminar combined forced and free convection heat transfer in a horizontal tube, *Int. J. Heat Mass Transfer* **10,** 1295–1309 (1969).
10. D. P. Siegwarth and T. J. Hanratty, Combined and experimental study of the effect of secondary flow on the temperature field and primary flow in a heated horizontal tube, *Int. J. Heat Mass Transfer* **13,** 27–42 (1970).
11. P. H. Newell and A. E. Bergles, Analysis of combined free and forced convection for fully developed laminar flow in horizontal tubes, *J. Heat Transfer* **92,** 83–93 (1970).
12. M. Van Dyke, Extended Stokes series: laminar flow through a heated horizontal pipe, *J. Fluid Mech.* **212,** 289–308 (1990).
13. C. A. Heiber and S. K. Sreenivasan, Mixed convection in an isothermally heated horizontal pipe, *Int. J. Heat Mass Transfer* **17,** 1137–1148 (1974).
14. J. W. Ou and K. C. Cheng, Natural convection effects on Graetz problem in horizontal isothermal tubes, *Int. J. Heat Mass Transfer* **20,** 953–960 (1977).
15. G. J. Hwang and M. J. Lin, Natural convection effects on laminar heat transfer in the thermal entrance region of horizontal isothermal tube, *J. Chinese Inst. Engrs* **8,** 343–355 (1985).
16. S. L. Lee, Weighting function scheme and its application on multidimensional conservation equations, *Int. J. Heat Mass Transfer* **32,** 2065–2073 (1989).
17. S. L. Lee, A new numerical formulation for parabolic differential equations under the consideration of large time steps, *Int. J. Numer. Meth. Engng* **26,** 1541–1549 (1988).
18. G. J. Hwang and K. C. Cheng, Boundary vorticity method for convective heat transfer with secondary flow application to the combined free and forced laminar convection in horizontal tubes, *Proc. 4th Int. Heat Transfer Conf.*, Versailles, Paris, Vol. **4,** Paper No. NC3.5 (1970).
19. C. A. Depew and R. C. Zenter, Laminar flow heat transfer and pressure drop with freezing at the wall, *Int. J. Heat Mass Transfer* **12,** 1710–1714 (1969).
20. G. J. Hwang and J. L. Chen, An experiment on combined laminar convection in an electrochemical flow system, *Chinese J. Mech.* **3**(1), 55–62 (1985).

APPENDIX

$$A_E = \frac{2F(a_{i+\frac{1}{2}}\Delta\phi)}{r_j^2(1-r_j^2)(\Delta\phi)^2}, \quad B_E = \frac{F(b_{i+\frac{1}{2}}\Delta\phi)}{r_j^2(\Delta\phi)^2}$$

$$A_W = \frac{2F(-a_{i-\frac{1}{2}}\Delta\phi)}{r_j^2(1-r_j^2)(\Delta\phi)^2}, \quad B_W = \frac{F(-b_{i-\frac{1}{2}}\Delta\phi)}{r_j^2(\Delta\phi)^2}$$

$$A_N = \frac{2F(a_{j+\frac{1}{2}}\Delta r)}{(1-r_j^2)(\Delta r)^2}, \quad B_N = \frac{F(b_{j+\frac{1}{2}}\Delta r)}{(\Delta r)^2}$$

$$A_S = \frac{2F(-a_{j-\frac{1}{2}}\Delta r)}{(1-r_j^2)(\Delta r)^2}, \quad B_S = \frac{F(-b_{j-\frac{1}{2}}\Delta r)}{(\Delta r)^2}$$

$$A_P = (A_E + A_W + A_N + A_S),$$

$$B_P = -(B_E + B_W + B_N + B_S)$$

$$B_R = -\left(\frac{\theta_N - \theta_S}{2(\Delta r)}\sin\phi_P + \frac{\theta_E - \theta_W}{2r_j(\Delta\phi)}\cos\phi_P\right), \quad b_R = \xi_P$$

where

$$F(Z) = [0, (1-0.1(|Z|)^5)] + [0, Z]$$

$[x, y]$: means maximum of x and y

$$a_{i+\frac{1}{2}} = r_j Ra\left(\frac{\psi_N - \psi_S + \psi_{EN} - \psi_{ES}}{4\Delta r}\right)$$

$$a_{i-\frac{1}{2}} = r_j Ra\left(\frac{\psi_N - \psi_S + \psi_{WN} - \psi_{WS}}{4\Delta r}\right) \qquad b_{i+\frac{1}{2}} = b_{i-\frac{1}{2}} = 0$$

$$a_{j+\frac{1}{2}} = \frac{1}{r_j + \frac{\Delta r}{2}}\left(1 - Ra\left(\frac{\psi_E - \psi_W + \psi_{EN} - \psi_{WN}}{4\Delta\phi}\right)\right) \qquad b_{i+\frac{1}{2}} = \frac{1}{r_j + \frac{\Delta r}{2}},$$

$$a_{j-\frac{1}{2}} = \frac{1}{r_j - \frac{\Delta r}{2}}\left(1 - Ra\left(\frac{\psi_E - \psi_W + \psi_{ES} - \psi_{WS}}{4\Delta\phi}\right)\right) \qquad b_{i-\frac{1}{2}} = \frac{1}{r_j - \frac{\Delta r}{2}}.$$